

EFFECT OF REYNOLDS NUMBER, OPERATING MODE, TURBULENCE PARAMETERS ON PROFILE AND SECONDARY LOSSES OF LPT

A.D. Nepomnyashchiy*, S.V. Suntsov*, S.Y. Danilkin*, V.P. Maslov*
*Central Institute of Aviation Motors (CIAM)

Keywords: *flat cascade, Reynolds number, turbulence*

Abstract

Two flat turbine cascades were experimentally investigated on an exhauster rig at low Reynolds numbers at different values of a flow's inlet turbulence intensity. The profile and the secondary losses obtained in flat cascades are represented as dependencies of a Reynolds number and a flow's inlet turbulence intensity. Some results of turbulence measurements are also presented in this paper.

1 Introduction

The negative effect of low Reynolds numbers is well known to reduce an efficiency of a Low Pressure Turbine (LPT). But not only low Reynolds numbers influence on a LPT's efficiency. Turbine operating modes and flow's inlet turbulence parameters could also impact on LPT's efficiency.

A LPT's efficiency decrease with Reynolds number occur due to growth of boundary layers and existence of separation flows in LPT's vane and blade rows.

In most of technical proceedings concerned impact of low Reynolds numbers on blade or vane losses isn't given an attention to influence of operating mode of a vane or a blade (isotropic reduced velocity at a blade's or vane's outlet). The effect of low Reynolds number is considered with a constant operating mode, for example [1], [2], [3]. As usual the operating mode equals to 0.6. Presented experimental results were obtained with relatively low flow's inlet turbulence intensity which is usually isn't higher than 0.045.

Some papers presents results of measurements of a turbulence intensity in a flow

part of model turbines, for example [4], [5], [6]. It is shown that turbulence intensity is growing in a turbine flow part from a turbine's inlet to a turbine's outlet and its averaged value could rise up to $Tu \sim 0.16$.

A low measured value of a turbulence intensity in a flow part of a LPT $Tu \sim 0.05$ is presented in paper [7]. These data should consider more attentively. The hot-wire probe DANTEC 55R01 with a diameter of the sensitive element of 70 μm was used to measure a turbulence intensity. To do correct measurements of flow's turbulence parameters the sensitive diameter of a hot-wire probe must be not higher than 5 μm .

The Paper presents the results of measurement the profile and the secondary losses in the two flat turbine cascades in a wide range of operating modes under various parameters of a flow's turbulence intensity at the cascades' inlet.

The main purpose of this and further such kind of experimental works is to develop ways of reducing the effect of low Reynolds number on profile and secondary losses of LPT's airfoils.

2 Exhauster Rig

The scheme of the experimental rig designed for the investigation of flat turbine cascades is shown on Fig. 1.

The experimental rig was constructed on an open scheme and operating on a cool atmospheric air on exhaust modes. The experimental rig consists of the inlet flaps, the adjustable throttle, the honeycomb and the turbulizing grid. The air is sucked from the atmosphere goes through the adjustable throttle,

then passes the honeycomb and flat turbine cascade towards the 3.8 MW compressor.

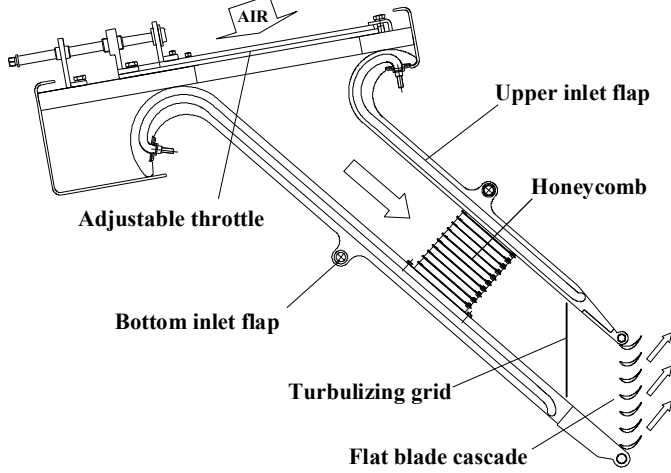


Fig. 1. The scheme of the experimental rig.

The adjustable throttle is needed to reduce the air's total pressure at the flat turbine cascade's inlet. The honeycomb and the inlet flaps align the airflow direction according to the constructive inlet angle of the flat turbine cascade.

The experimental rig provides an independent control of the inlet total pressure and operating mode of a flat turbine cascade. The experimental rig allows to carry out the investigation in the wide range of the operating modes $\lambda_{is} = 0.3 - 1.20$ and the total pressure at the cascade's inlet of $p_0^* = 0.15 - 0.9$ bar.

Here and below the operating mode of a flat turbine cascade is calculated using following equation:

$$\lambda_{is} = \sqrt{\frac{k+1}{k-1} \cdot \left(1 - \left[\frac{p_2}{p_0^*} \right]^{\frac{k-1}{k}} \right)} \quad (1)$$

where

p_0^* – the averaged total pressure at the cascade's inlet;

p_2 – the averaged static pressure at the cascade's outlet;

k – the isentropic exponent of an air.

The experimental investigations were performed with and without the turbulizing grid located behind the honeycomb before flat cascades, see Fig. 1.

3 Cascades' Parameters

Some geometrical parameters of the two flat turbine cascades are presented in the Table 1.

Table 1 Geometrical parameters of the turbine cascades

	β_{1c}	β_{2eff}	\bar{C}_m	\bar{t}	δ	\bar{d}_1	\bar{d}_2
1	53.4	22.8	0.158	0.739	9.1	0.033	0.035
2	48.8	33.5	0.128	0.710	21.3	0.031	0.035

where

β_{1c} – the designed inlet angle of the blade in the cascade, degree;

β_{2eff} – the effective outlet angle calculated as the arcsin from the ratio between the cascade's throat and the cascade's blades pitch, degree;

\bar{C}_m – the ratio between the profile's maximum thickness to the blade chord;

\bar{t} – the non-dimensional pitch defined as the ratio between the cascade's blades pitch to the blade's chord;

δ – unguided turning angle, degree;

\bar{d}_1 – the ratio between the leading edge's diameter to the blade's chord;

\bar{d}_2 – the ratio between the trailing edge's diameter to the cascade's throat.

In the Table 1 and below the cascades' angles and flow's angles are counted from the front of the flat cascade.

The first cascade was designed to operate at the transonic operating modes of $\lambda_{is} = 0.9 - 1.05$ at the Reynolds numbers of $Re = 2 \cdot 10^5 - 3 \cdot 10^5$ (here and below Reynolds number Re is calculated on a blade chord and isotropic flow parameters at the cascade's outlet). The main feature of this cascade is a low value of the unguided turning angle.

The second cascade was designed to operate at the subsonic operating modes of $\lambda_{is} = 0.55 - 0.65$ at the Reynolds numbers of $Re = 0.7 \cdot 10^5 - 0.8 \cdot 10^5$. The main features of this cascade are a high value of unguided turning angle and a low confuser of the cascade's flow part.

The each flat turbine cascade consists of 7 blades. The blades' chord in the cascades is 40 mm. The ratio between the blades' length and the blades' chord in both cascades is 3.0.

4 Instrumentation

The total pressure, the pressure, the flow velocity, the yaw angle (the angle between center-line of the rig's flow part and the flow velocity component along the blades' height) and the pitch angle (the angle between center-line of the rig's flow part and the flow velocity component along the blades' pitch) were measured at the flat cascade's inlet and at outlet by means of the five-hole pressure probes. The errors of pressure acquisition for each channel of the five-hole pressure probes were not higher than 0.25%. The two five-hole pressure probes had previously been calibrated in a calibration nozzle before the investigations.

The five-hole pressure probes were able to traverse both along the blades' pitches and along the blades' height. The parameters of the flow were measured on the cascade's stationary operating modes with the acquisition frequency of 10 Hz during movement of the five-hole pressure probes along the blades' pitches at the constant blades' height. The averaging of the flow parameters such as the total pressure, the pressure, the yaw angle and the pitch angle were performed per one blades' pitch for the each stationary operating mode.

The turbulence intensity and the velocity power spectrum at the cascade's inlet were measured by means of the fast-response pressure probe Kulite FAP-HT-250 [8], [9]. The fast-response pressure probe had been calibrated in the calibration nozzle before it was used in the experimental investigation of the flat cascades. The data obtained by means of the fast-response pressure probe in the calibration nozzle were compared with the data obtained by means of the hot-wire probe DANTEC CTA 56C17 at the same conditions.

The measured averaged reduced velocity in the calibration nozzle by means of the fast-response pressure probe and the hot-wire probe are shown on Fig. 2.

Here and below the reduced velocity is calculated as the ratio between the flow velocity and the critical velocity of a sound a_{cr} . The critical velocity of a sound is calculated by following equation:

$$a_{cr} = \sqrt{\frac{2 \cdot k}{k + 1} \cdot R \cdot T_0^*} \quad (2)$$

where

T_0^* – the total temperature of a flow;

R – the gas constant of an air.

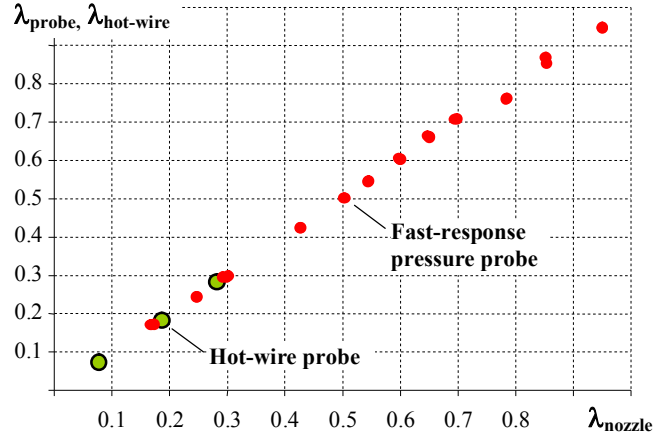


Fig. 2. The measured averaged reduced velocities in the calibration nozzle.

where

λ_{probe} - the averaged reduced velocity measured by means of the fast-response pressure probe;

$\lambda_{hot-wire}$ - the averaged reduced velocity measured by means of the hot-wire probe;

λ_{nozzle} - the averaged reduced velocity of a flow in the calibration nozzle (operating mode of the nozzle).

The turbulence intensity of the flow velocity axial component versus the operating mode of the calibration nozzle's is shown on Fig. 3.

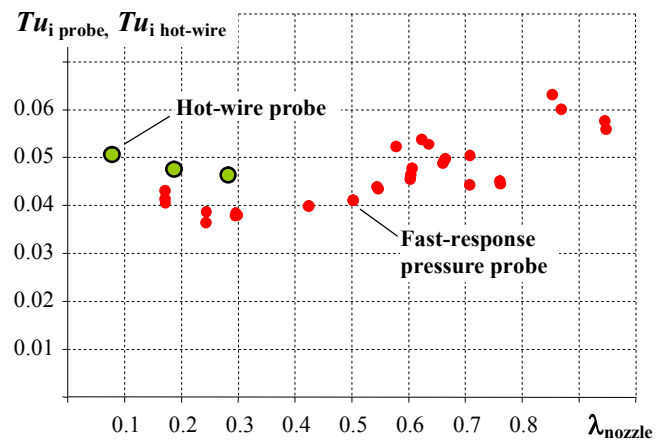


Fig. 3. The turbulence intensity of the flow velocity axial component in the calibration nozzle.

where

$Tu_{i\ probe}$ - the turbulence intensity of the flow velocity axial component measured by means of the fast-response pressure probe;

$Tu_{i\ hot-wire}$ - the turbulence intensity of the flow velocity axial component measured by means of the hot-wire probe.

The power spectra of the flow velocity axial component in the calibration nozzle on the operating mode of $\lambda_{nozzle} \sim 0.29$ received using the fast-response pressure probe and the hot-wire probe are shown on Fig. 4.

Power spectra were calculated using the Fast Fourier Transformation algorithm for the flow velocity axial component. The obtained power spectra are satisfying the following equation:

$$u'^2 = \int_0^{\infty} E df \quad (3)$$

where

E – the power spectrum of a flow velocity component, m^2/c ;

f – the frequency, Hz;

u'^2 – the root mean square (RMS) of a flow velocity component, m^2/c^2 .

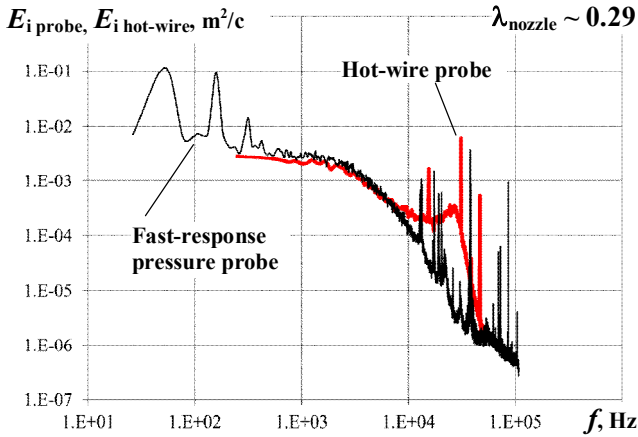


Fig. 4. The power spectra of the flow velocity axial component in the calibration nozzle.

where

$E_{i\ probe}$ – the power spectrum of the flow velocity axial component measured by means of the fast-response pressure probe, m^2/c ;

$E_{i\ hot-wire}$ – the power spectrum of the flow velocity axial component measured by means of the hot-wire probe, m^2/c .

It is seen on Fig. 4 that the operating mode of the calibration nozzle wasn't strictly

stationary due to the presence of peaks at the low frequency part of the power spectrum. To avoid mistakes in calculation of flow's turbulence parameters the almost all obtained power spectra were filtered. The initial and the filtered power spectra of the flow velocity axial component in the calibration nozzle on the operating mode of $\lambda_{nozzle} \sim 0.29$ received using the fast-response pressure probe are shown on Fig. 5.

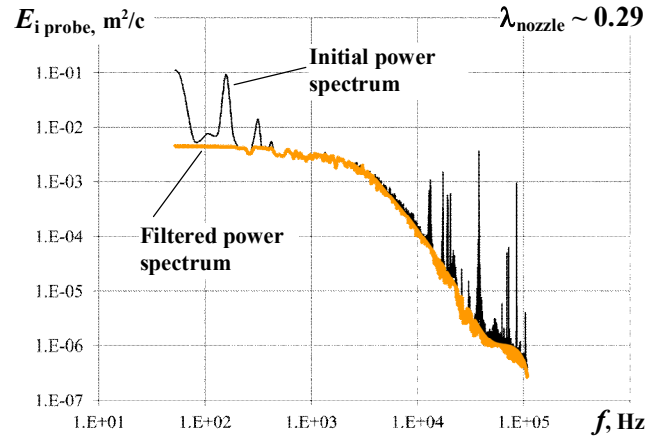


Fig. 5. The initial and the filtered power spectra of the flow velocity axial component in the calibration nozzle.

5 Results and Discussion

5.1 Profile and Secondary Losses Measurements

The profile losses in the first flat cascade (see Table 1) versus the operating mode at the different total pressure of a flow at the cascade's inlet are shown on Fig. 6.

The profile losses were calculated using the measured at the blades' mid height averaged total pressure at the cascade's inlet p_0^* and outlet p_2^* and the averaged pressure at the cascade's outlet p_2 as follows:

$$\lambda_2 = \sqrt{\frac{k+1}{k-1} \cdot \left(1 - \left[\frac{p_2}{p_2^*} \right]^{\frac{k-1}{k}} \right)} \quad (4)$$

$$\zeta_{pr} = 1 - \left(\frac{\lambda_2}{\lambda_{is}} \right)^2 \quad (5)$$

where

p_2^* - the averaged total pressure at the cascade's outlet;

λ_2 - the averaged reduced velocity at the cascade's outlet;

λ_{is} - the operating mode, see (1).

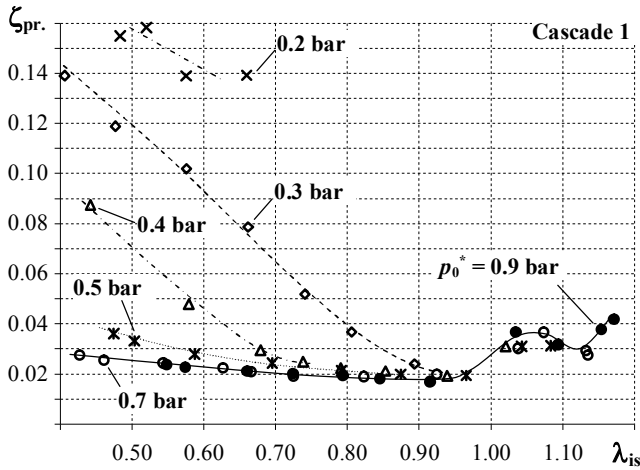


Fig. 6. The profile losses versus the operating mode in the first flat cascade.

As it seen on Fig. 6, the profile losses are splitting up with the decrease of the operating mode and the total pressure at the cascade's inlet.

The same profile losses were recalculated as a function of the Reynolds number as it's shown on Fig. 7. The profile losses obtained with higher turbulence intensity at the cascade's inlet generated by means of a grid are also plotted on Fig. 7.

As it seen on Fig. 7, the influence of the operating mode and the total pressure at the cascade's inlet expresses as a function of only the Reynolds number.

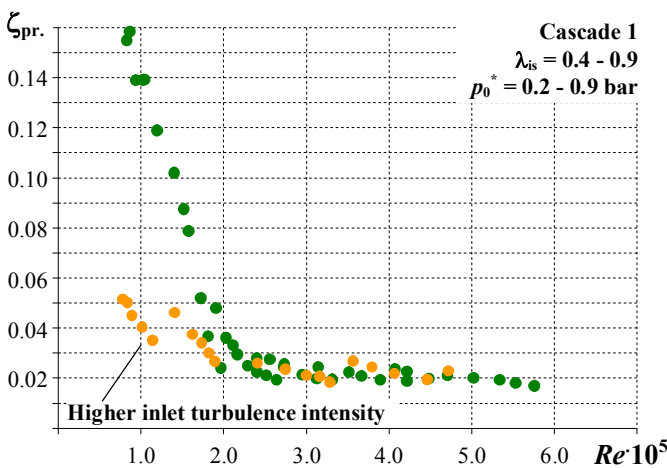


Fig. 7. The profile losses versus the Reynolds number in the first flat cascade.

As mentioned above, the first cascade was optimally designed with lower value of the unguided turning angle to operate at the transonic operating modes at the Reynolds numbers of $Re = 2 \cdot 10^5 - 3 \cdot 10^5$. Probably that's why we see the dramatically growth of the losses in the cascade at the $Re < 2 \cdot 10^5$. Higher turbulence intensity could slow down the growth of the losses.

The profile losses versus the Reynolds number in the second cascade (see Table 1) are plotted on Fig. 8. The profile losses obtained in the second flat cascade with dimples located on the blades' suction sides are also plotted on Fig. 8.

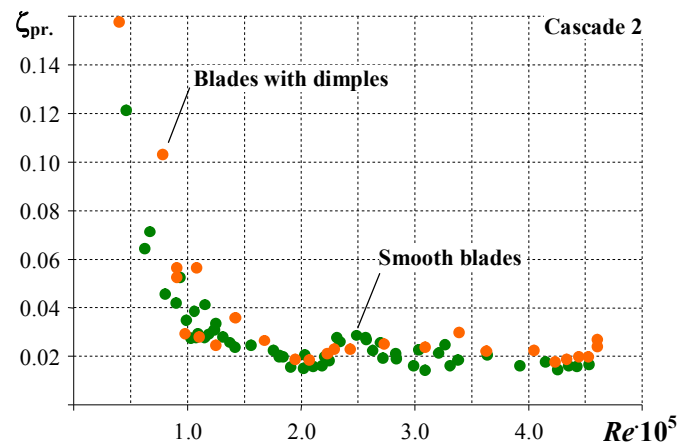


Fig. 8. The profile losses versus the Reynolds number in the second flat cascade.

The photo of the cascade's blade with dimples is shown on Fig. 9.

The profile losses versus the Reynolds number in the second flat cascade with the smooth blades and the blades with dimples obtained at higher inlet turbulence intensity at the cascade's inlet generated by means of a grid are plotted on Fig. 10.

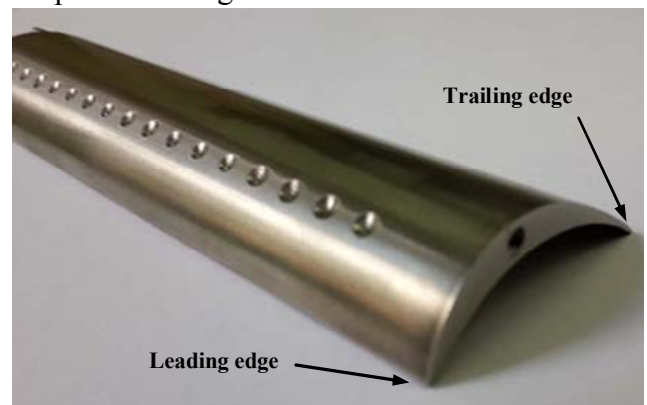


Fig. 9. The photo of the cascade's blade with dimples.

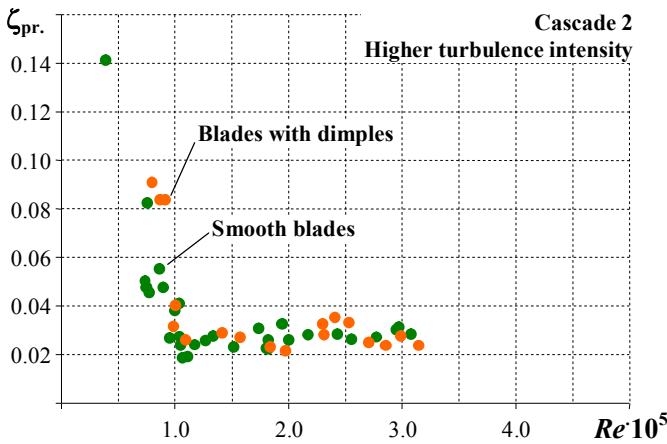


Fig. 10. The profile losses versus the Reynolds number at higher inlet turbulence intensity in the second flat cascade.

The dependencies of the profile losses on the Reynolds number shown on Fig. 8 and on Fig. 10 were obtained at the operating modes in the range of $\lambda_{is} = 0.3 - 0.85$ and the total pressure at the cascade's inlet in the range of $p_0^* = 0.2 - 0.8$ bar.

The Fig. 8 and the Fig. 10 show that higher turbulence intensity has led to increase in the profile losses in the second cascade by ~ 0.01 at the $Re > 1.5 \cdot 10^5$. The dependencies of the profile losses on the Reynolds number are the same for the both cases at the $Re < 1.0 \cdot 10^5$, see Fig. 8 and Fig. 10. The same pattern of no effect of the inlet turbulence intensity on the profile losses in flat cascades at low Reynolds numbers are presented in [10].

The characteristics of the second flat cascade with the smooth blades and the blades with dimples haven't any differences, see Fig. 8 and Fig. 10 "Blades with dimples". Probably this takes place due to a location of dimples in a front part of blades' suction sides far from the narrow section of the blades' channel (or blades' throat), see Fig. 9.

It's assumed that a growth of the profile losses at low Reynolds numbers occur due to an appearance of a flow separation on blades' suction sides near trailing edges. An emergence of a flow separation as a function of Reynolds number depends on the geometrical parameters of the flat cascade and on the inlet flow parameters, see Fig. 7. It should be noted that growth of the profile losses on the Reynolds number in different cascades could be close in

some conditions, see Fig. 7 "Higher inlet turbulence intensity" and Fig. 8.

As mentioned above the profile losses were calculated using the flow parameters measured at the blades' mid height far away from zones of secondary flows appearing near the end walls of the cascades. Although the flat cascades consists of the blades with the same geometry along its height it's also helpful to know a behavior of the secondary flows on the Reynolds number.

The losses in the second flat cascade along the blades' height obtained without using the turbulizing grid at the operating mode of $\lambda_{is} = 0.6$ are shown on Fig. 11.

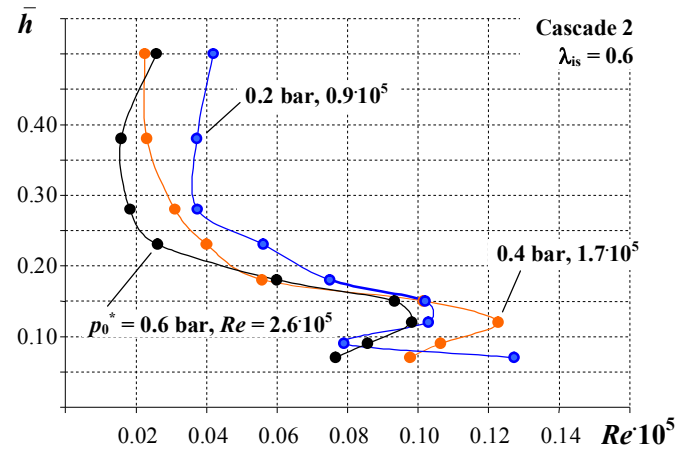


Fig. 11. The losses in the second flat cascade along the blades' height.

The vertical axis \bar{h} on the Fig. 11 is the reduced blade height (0 - is a blades' hub, 1 - is a blades' tip).

The averaged pitch angles of a flow at the second cascade's outlet along the blades' height obtained without using the turbulizing grid at the operating mode of $\lambda_{is} = 0.6$ are shown on Fig. 12.

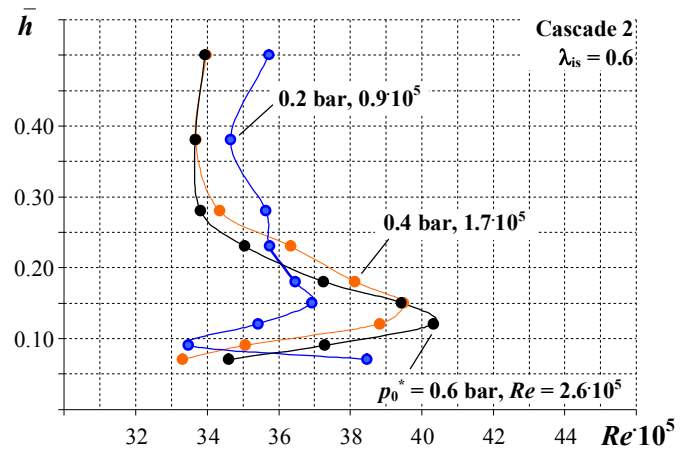


Fig. 12. The averaged pitch angles of a flow at the second cascade's outlet.

As it's seen from the Fig. 11 and Fig. 12 the quarter of the blades' height from the end wall is occupied by the secondary flows. Fig. 11 also shows that the losses in the secondary flows don't change on the Reynolds number.

The same behavior of the secondary losses on the Reynolds number was obtained in the second cascade with using the turbulizing grid.

5.2 Turbulence Measurements

As mention above the turbulence measurements were performed at the cascade's inlet by means of the fast-response pressure probe Kulite FAP-HT-250.

The turbulence measurements were performed at the mid height of the cascade's blades along almost four blade's pitches with the turbulizing grid mounted ahead of the cascade and without the turbulizing grid. The turbulence intensity of the flow velocity axial component at the cascade's operating mode of $\lambda_{is} = 0.65$ at the different values of the inlet total pressure are plotted on Fig. 13 and on Fig. 14.

The turbulence intensity of the flow velocity axial component versus the Reynolds number obtained in the wide range of the cascade's operating modes $\lambda_{is} = 0.3 - 0.85$ and in the range of the inlet total pressure $p_0^* = 0.2 - 0.8$ bar are plotted on Fig. 15.

It's seen from Fig. 15 that the data obtained at the different flow parameters expresses as the function of the Reynolds number. The scatter of the turbulence intensity on the Reynolds number observed with the turbulizing grid probably occurred due to unsteady flow behind the grid in a measurements location.

The turbulence intensity in the flow part of the experimental rig is generated by the honeycomb and by the turbulizing grid. The observed growth of the turbulence intensity with reducing the Reynolds number (see Fig. 15 "Without the turbulizing grid") could be explained by a decrease of the turbulence dissipation in low density flows [11].

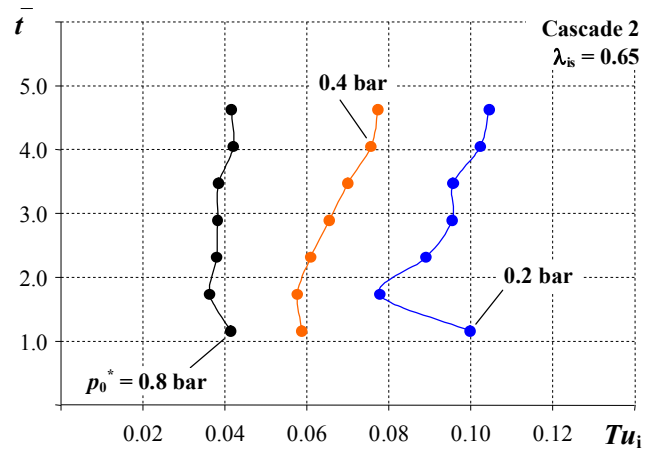


Fig. 13. The turbulence intensity of the flow velocity axial component at the cascade's inlet without the turbulizing grid.

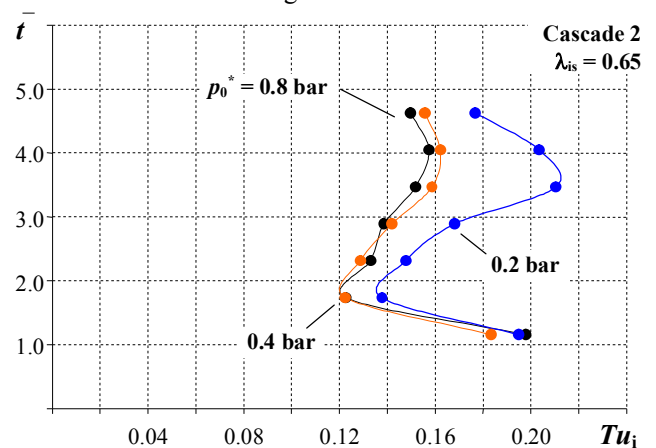


Fig. 14. The turbulence intensity of the flow velocity axial component at the cascade's inlet behind the turbulizing grid.

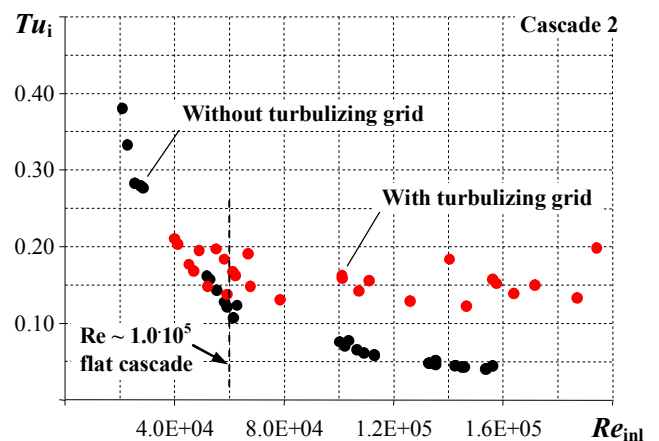


Fig. 15. The turbulence intensity of the flow velocity axial component at the cascade's inlet versus the Reynolds number.

where

\bar{t} – the non-dimensional pitch, see above;

Tu_i – the turbulence intensity of the flow velocity axial component;

Re_{inl} – the Reynolds number calculated on the flow parameters at the cascade's inlet using the characteristic size of 40 mm.

6 Conclusion

Two flat turbine cascades were experimentally investigated on the exhauster rig at low Reynolds numbers at different values of the inlet turbulence intensity. The investigation were carried out in the wide range of the cascades' operating modes $\lambda_{is} = 0.3 - 0.85$ and in the range of the inlet total pressure $p_0^* = 0.2 - 0.9$ bar. The investigation showed the following:

- The profile losses in the flat cascades are the function of the Reynolds number and the inlet turbulence.
- The profile losses in the flat cascades dramatically increase from the certain Reynolds number, which is associated with the emergence of a flow separation on the blades' suction sides.
- The high level of turbulence intensity could decrease the profile losses at low Reynolds numbers but it also could increase the losses at higher Reynolds numbers.
- The secondary losses don't change on Reynolds numbers at the same operating mode ($\lambda_{is} = \text{const}$). The secondary losses are expected to be decrease with rising the cascade's operating mode.
- The dimples located on the suction sides of blades probably could minimize the profile losses at low Reynolds numbers because of reducing a flow separation [12]. But difficult to expect the reducing losses at low Reynolds numbers if dimples located in front part of blades' suction side as in present investigation.
- The turbulence intensity at the cascade's inlet is a function of the Reynolds number. The change of the inlet turbulence intensity on the Reynolds number is correlated with the change of the profile losses on the Reynolds number. The growth of the turbulence intensity probably occurs due to

decrease of the turbulence dissipation in low density flows.

- The test conditions of flat cascades are close to operating conditions of LPT's blade or vane rows in terms of Reynolds numbers. Obtained results of model tests of flat cascades could be applied to LPT's blade or vane rows if the turbulence parameters of a flow at the cascades' inlets in the experimental investigation corresponded to engine's operating conditions of a LPT.
- Results of flat turbine cascades' investigation are particularly relevant for developing and verification of CFD methods of LPT at low Reynolds numbers.

References

- [1] Parkash C., Cherry D.G., Shin H.W., Machnaim J., Dialely L., Beacock R., Halstead D., Wadia A.R., Guillot S., Ng W.F. Effect of Loading Level and Distribution on LPT Losses. *ASME Paper*, GT2008-50052, 2008.
- [2] Martinstetter M., Niehuis R., Franke M. Passive Boundary Layer Control on a Highly Loaded Low Pressure Turbine Cascade. *ASME Paper*, GT2010-22739, 2010.
- [3] Michálek J., Monaldi M., Arts T. Aerodynamic Performance of a Very High Lift Low Pressure Turbine Airfoil (T106C) At Low Reynolds And High Mach Number With Effect Of Free Stream Turbulence Intensity. *ASME Paper*, GT2010-22884, 2010.
- [4] Zaccaria M., Lakshminarayana B. An Experimental Investigation of Steady and Unsteady Flow Field in an Axial Flow Turbine. *NASA*, CR-4778, 1997.
- [5] Göttlich E., Marn A., Pecnik R., Malzacher F.J., Schennach O., Pirker H.P. The Influence of Blade Tip Gap Variation on the Flow Through an Aggressive S-Shaped Intermediate Turbine Duct Downstream a Transonic Turbine Stage - Part II: Time-Resolved Results and Surface Flow. *ASME Paper*, GT2007-28069, 2007.
- [6] Matsunuma T., Tsutsui Y. Effect of Low Reynolds Number on Wake-Generated Unsteady Flow of an Axial-Flow Turbine Rotor. *International Journal of Rotating Machinery*, Issue 1, pp 1 – 15, 2005.
- [7] Binder A., Schroeder Th., Hourmouziadis J. Turbulence Measurements in a Multistage Low-Pressure Turbine. *Journal of Turbomachinery*, Vol. 111, pp 153-161, 1989.

- [8] Flow angle probe high temperature miniature is pressure transducer FAP-HT-250 series. URL: <http://www.kulite.com/docs/products/FAP-HT-250.pdf>.
- [9] Nepomnyashchiy A.D., Turbulence Measurements in a Flow Part of Turbomachines Using a High-Frequency Pressure Probe. *ICAS paper*, ICAS2014-7.4.3-2014_0252, 2014.
- [10] Hoheisel H., Kiock R., Lichtfuss H.J., Fottner L. Influence of Free-Stream Turbulence and Blade Pressure Gradient on Boundary Layer and Loss Behavior of Turbine Cascades. *ASME J. Turbomachinery*, Vol. 109, No. 2, pp 210-219, 1987.
- [11] Hinze J.O., *Turbulence*. McGraw-Hill, 1st edn, 1959.
- [12] Casey J.P., Effect of Dimple Pattern on the Suppression of Boundary Layer Separation on a Low Pressure Turbine Blade. *Master's Thesis*, AFIT/GAE/ENY/04-M05, 2004.

Copyright Statement

The authors confirm that they, and/or their company or organization, hold copyright on all of the original material included in this paper. The authors also confirm that they have obtained permission, from the copyright holder of any third party material included in this paper, to publish it as part of their paper. The authors confirm that they give permission, or have obtained permission from the copyright holder of this paper, for the publication and distribution of this paper as part of the ICAS proceedings or as individual off-prints from the proceedings.

Contact Author Email Address

Mail to: nepomnashi@ciam.ru
nepomnashi@gmail.com